Chemistry - Methods

Chemistry—Methods

Chemistry Europe
European Chemical Societies Publishing

RESEARCH ARTICLE OPEN ACCESS

Supramolecular Aggregates of Amino Acid-Functionalized 1,8-Naphthalimides for Chiral Recognition

Salvatore Marullo | Francesca D'Anna

Dipartimento di Scienze e Tecnologie Biologiche Chimiche e Farmaceutiche, Università degli Studi di Palermo, Palermo, Italy

Correspondence: Francesca D'Anna (francesca.danna@unipa.it)

Received: 6 March 2026 | **Revised:** 22 May 2026 | **Accepted:** 30 May 2026

Keywords: chiral recognition | fluorescent sensing | self-assembly

ABSTRACT

Methods for fast enantioselective recognition hold relevance in several fields of chemical research. In this context, we studied the chiral recognition ability of fluorescent supramolecular aggregates formed in solution by chiral, amino acid-functionalized 1,8-naphthalimide derivatives, namely **L-Phe-NI**, **L-Ala-NI**, and **D-Ala-NI**. First, we studied the photophysical properties of the fluorophores and their self-assembly process, by concentration- and temperature-dependent UV–vis and fluorescence spectroscopy, finding that aggregation follows different pathways, isodesmic or cooperative, depending on the functionalization of the imide position. Subsequently, we investigated the chiral recognition ability of the aggregates formed in acetonitrile solutions, toward enantiomeric pairs of aromatic alcohols and amines, such as 1-phenylethanol, 1-phenetylethylamine, 1-(2-naphthyl)-ethanol, and 1-(2-naphthyl)-ethylamine by fluorescence and resonance light scattering measurements. We found that aggregates of **L-Ala-NI** exhibited the highest chiral discrimination. Notably, we demonstrated that these aggregates can be embedded onto solid supports like filter paper strips or polymer films, maintaining their chiral recognition ability.

1 | Introduction

Chirality is a ubiquitous phenomenon in nature, across very different scales, from nucleic acids and cells to galaxies [1]. In the chemical field, the possibility to distinguish, separate, or recognize the single components of enantiomeric pairs, for example, to establish the enantiomeric composition of a mixture, has key implications in a broad range of application fields, from medicinal chemistry to nonlinear optics and separations, to name a few [2, 3]. Chiral recognition events therefore, imply the occurrence of a significantly different interaction between a chiral probe and the individual components of a given enantiomeric pair, eliciting a distinct and different response. To date, several different techniques have been successfully developed to this purpose, such as UV–vis and fluorescence spectroscopy [4], circular dichroism [5], NMR spectrometry [6, 7], or chiral HPLC [8]. In this context, fluorimetric methods for chiral recognition have recently garnered considerable interest owing to fast response, high sensitivity, and cost-effectiveness [9, 10].

Regarding the probes that can be used as chiral reporters, recent years have witnessed an increase in interest toward chiral supramolecular aggregates [2, 11]. Underpinned solely by non-covalent interactions, chirality in self-assembled systems can be achieved either by helical self-association of achiral molecules or by supramolecular polymerization of chiral small molecules [1]. Consequently, emissive chiral supramolecular polymers can show significant ability of chiral recognition, when the individual components perturb the emission of the aggregates by either emission quenching or enhancement differently. Among the fluorescent supramolecular aggregates with sensing capability, we have recently shown that derivatives of 1,8-naphthalimide, substituted at both the imide- and core position, can act as fluorescent sensors for pharmaceutically active compounds, showing sub-micromolar limits of detection [12, 13].

In addition, host-guest complexes of 1,8-naphthalimide derivatives with cucurbit[7]uril have shown chiral discrimination between the enantiomers of amino acids [14]. Supramolecular aggregates of 1,8-naphthlaimide functionalized luminogens have been employed as systems showing circularly polarized luminescence [15, 16], helicity tuning [17], as well as intramolecular charge transfer (ICT) when tethered to donor π-conjugated moieties [18]. Thus, emissive supramolecular aggregates obtained from chiral 1,8-naphthalimide-derivatives could, in principle, exhibit chiral recognition ability.

Based on these considerations, herein we synthesized three chiral 1,8-naphthalimide fluorescent derivatives, namely **L-Phe-NI**, **L-Ala-NI**, and **D-Ala-NI**, as reported in Figure 1.

In particular, these chiral fluorophores are functionalized at the imide position with amino acid residues, deriving from L-phenylalanine and the enantiomeric L- and D-alanine. Hence, the fluorophores synthesized can interact both by π–stacking interactions and through hydrogen bonds. Regarding the aromatic core, it is widely reported in the literature that substitution at the aromatic ring, especially at the 4-position, can enhance fluorescence in 1,8-naphthalimides compared with the unsubstituted analog, and the presence of a chlorine atom can increase the acceptor character of the fluorophore [19, 20].

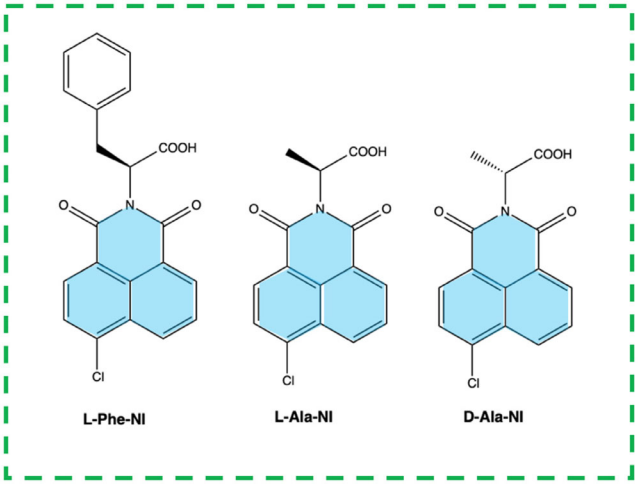

FIGURE 1 | Structures of 1,8-naphthalimide derivatives used in this work.

Accordingly, 4-halo substituted 1,8-naphthalimides have been employed as fluorescent sensors for different analytes [13, 21]. Initially, we studied their photophysical properties by solvent-dependent UV–vis and fluorescence measurements. In addition, we determined the relative fluorescence quantum yield in selected solvents. Then, we investigated the self-assembling ability of each fluorophore in the aggregation supporting solvents like acetonitrile and water, by concentration- and temperature-dependent UV–vis and fluorescence measurements, to elucidate the aggregation mechanism as well as the stability of the aggregates and the thermodynamic features of the aggregation process. Finally, we explored the possibility of using the aggregates in solution as a chiral recognition platform, toward chiral "guest" molecules, namely (*R*)- and (*S*)-1-phenylethanol (PhEtOH), (*R*)- and (*S*)-1-phenetylethylamine ($PhEtNH_2$), (*R*)- and (*S*)-1-(2-naphthyl)-ethanol (NaphEtOH) and (*R*)- and (*S*)-1-(2-naphthyl)-ethylamine ($NaphEtNH_2$), reported in Figure 2.

These chiral molecules bear both hydrogen bond donor groups and aromatic rings. Therefore, they can in principle interact with the fluorophores through noncovalent interactions such as hydrogen bonding and π-stacking. In addition, they differ not only for their chirality, but also for the number of hydrogen bonding donor sites and for the π-surface area, which may affect the overall interaction with the fluorescent probes. The chiral recognition ability was evaluated by fluorescence and resonance light scattering (RLS) measurements, whereas the interaction mode between the fluorophores and selected chiral guests was investigated by ^1H NMR. Finally, we assessed the possibility of chiral recognition also in solid phases, by embedding the best-performing probe, **L-Ala-NI**, on solid supports such as paper strips and poly-(3-hydroxybutirate) polymer films.

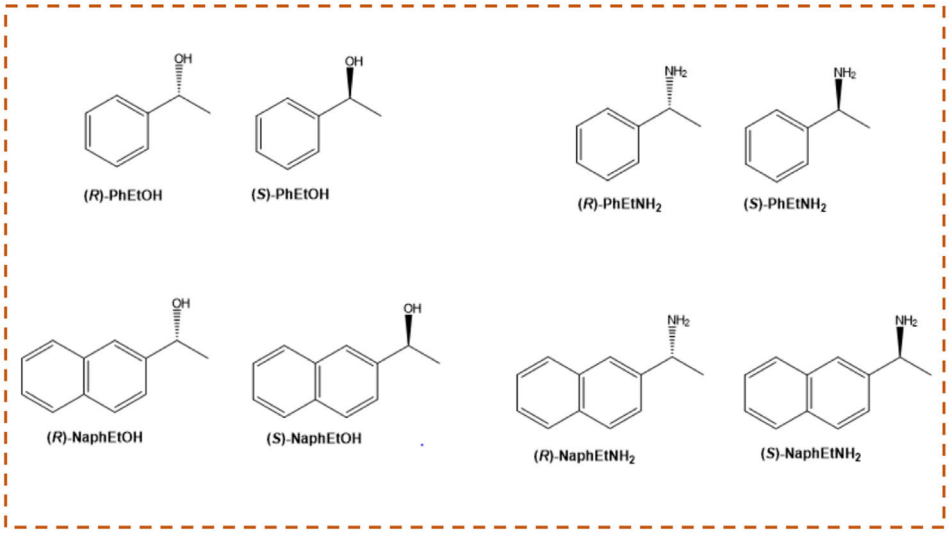

FIGURE 2 | Structures of chiral guest molecules used in chiral recognition tests.

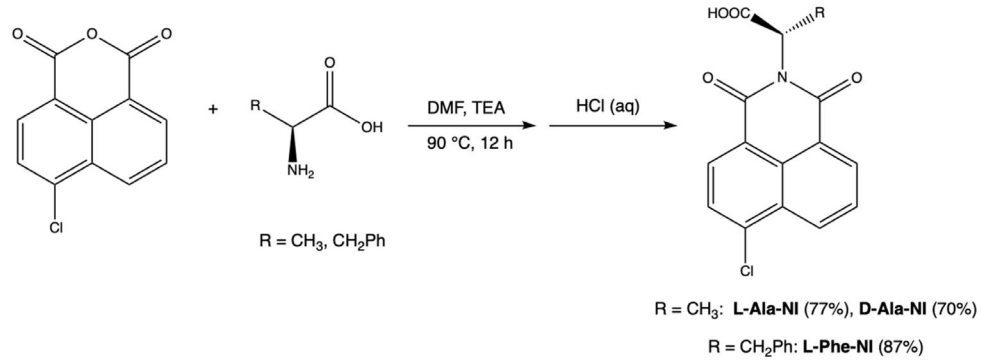

FIGURE 3 | Synthesis of the fluorophores.

2 | Results and Discussion

2.1 | Synthesis of Fluorophores

All the fluorophores were prepared according to a reported procedure [22], by reacting 4-chloro-1,8-naphthalimide with the suitable amino acid in DMF, in the presence of triethylamine, followed by the addition of hydrochloric acid as reported in Figure 3, yielding the fluorophores in good to high yield, comprised between 70% and 87%.

2.2 | Photophysical Properties of the Fluorophores

Preliminary investigation of the photophysical properties of the fluorophores was carried out by solvent-dependent UV–vis and fluorescence measurements. To this aim, we recorded the UV–vis and fluorescence spectra of solutions containing a fixed concentration of fluorophores, in different solvents, spanning a wide range of polarity, either protic or aprotic. Representative spectra, relevant to **L-Phe-NI,** are shown in Figure 4,

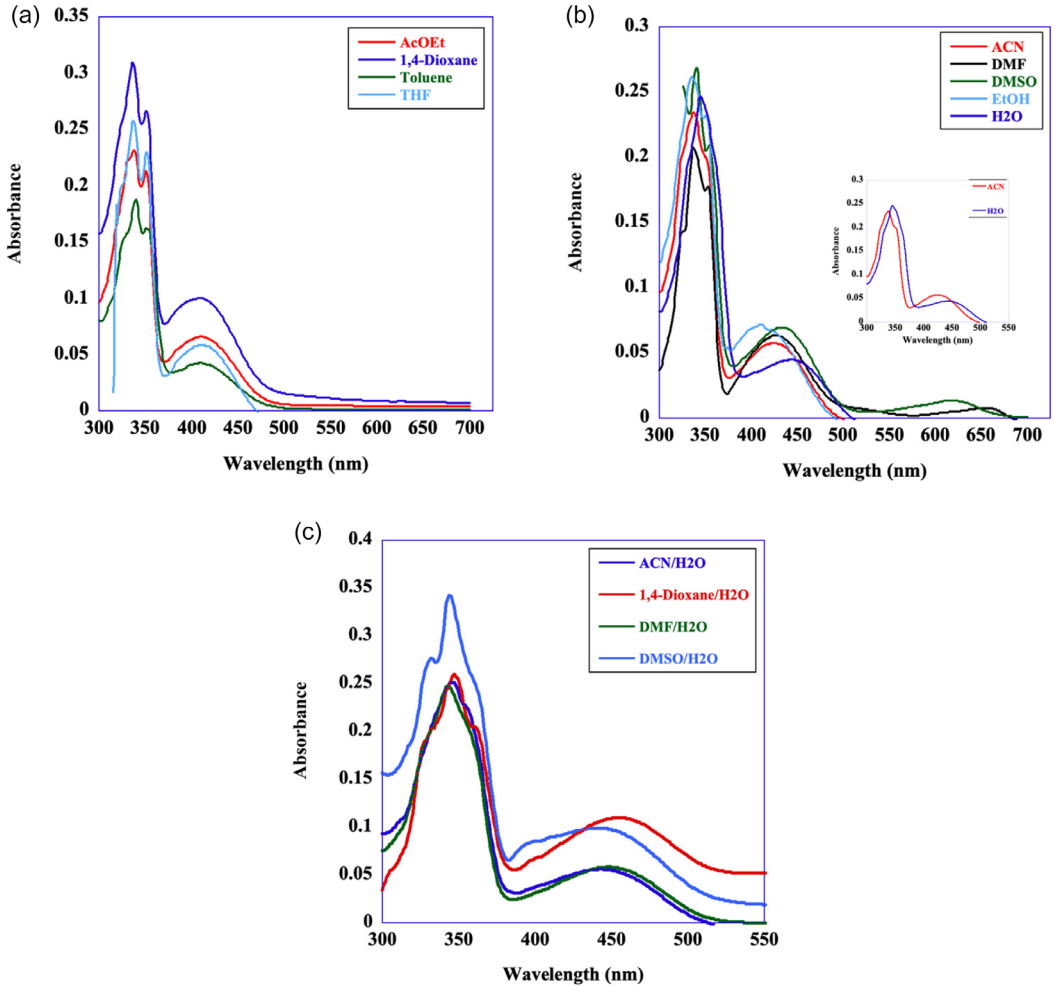

FIGURE 4 | Superimposed UV–vis spectra of **L-Phe-NI** ($2.8 \cdot 10^{-5}$ M) in (a) apolar aprotic solvents, (b) polar solvents, ACN and H_2O in the inset and (c) binary aqueous solvent mixtures.

while the ones obtained for the other fluorophores are reported in Figure S1.

In general, the spectra reported in Figure 4 feature two main absorption bands, the most intense centered around 340 nm, while the other one is rather broad, centered in the range between 410 and 440 nm. In particular, as reported in the literature, the former band can be ascribed to π–π* transitions from the aromatic core [20], and as reported in Table S1, its position shifts to higher wavelengths as solvent polarity increases from 337 nm in 1,4-dioxane to 345 nm in water, suggesting a positive solvatochromism, which has been previously observed for different 1,8-naphthalimide derivatives [23]. In addition, while in apolar solvents (Figure 4a), this band shows a clear fine structure, which is lost in solutions of more polar solvents, like acetonitrile and water, as shown in the inset in Figure 4b. This finding could suggest the formation of supramolecular aggregates in these solvents [12, 24].

Notably, the same loss in fine structure occurs in mixtures of water with other solvents, as reported in Figure 4c. The higher wavelength absorption could derive from a charge transfer band [20], and its position is less sensitive to solvent polarity. Similar conclusions can be drawn for **L-Ala-NI**, whose spectra are reported in Figure S1 and Table S1. In this case, all spectra show the occurrence of a single band, centered between 330 and 345 nm. Once again, this band loses its fine structure in water and, to a lesser extent, in acetonitrile, while $_{max}$ undergoes a bathochromic shift as the solvent polarity increases.

With the same approach, we obtained the fluorescence emission spectra, reported in Figure 5 for **L-Phe-NI** and in Figure S2 for **L-Ala-NI**.

Observing the spectra reported in Figure 5a shows that in low or medium-polarity aprotic solvents, the emission spectra are characterized by two bands, centered at 400 and 500 nm, with the only exception of acetone, in which only the former is present. On the other hand, as shown in Figure 5b, in protic or highly polar solvents, a single band is present, located at 400 nm in EtOH and ACN, or 440 nm in water. Emission is practically quenched in DMSO and DMF, with a weak emission band centered at 500 and 530, respectively. A similar approach was employed to elucidate the emission properties of **L-Ala-NI** as a function of the solvent, obtaining the spectra reported in Figure S2. Once again, the emission spectra in lower polar solvents, like dichloromethane, chloroform, THF, and dioxane, with the only exception of toluene, show a single band centered around 400 nm (Figure S2a), with a fine structure that is lost in higher polar or protic solvents, as shown in Figure S2b. In this latter case, emission is entirely quenched in solvents like DMF and DMSO, whereas a significant emission is displayed in ACN, ethanol and water. Notably, the emission spectrum keeps its features also when water is mixed with 10 vol% of organic cosolvents, as shown in Figure S2c. However, for **L-Ala-NI**, no obvious correlation could be found between λ_{max} and the polarity of the solvent, as expressed by the relative dielectric constant. Based on these considerations, we hypothesize that also for **L-Ala-NI**, water and ACN could be aggregation-supporting solvents. To further investigate the possible supramolecular aggregation of both fluorophores, we carried out concentration-dependent UV–vis and fluorescence measurements in a solution of water and ACN.

2.3 | Concentration-Dependent UV–Vis and Fluorescence Investigation

First, to investigate the possible self-assembly, and to elucidate the nature of the aggregates formed, we initially carried out concentration-dependent UV–vis measurements for both fluorophores in water and acetonitrile. The spectra obtained for **L-Phe-NI** are reported in Figure 6, while the ones relevant to **L-Ala-NI** are shown in Figure S3.

Examining the spectra reported in Figure 6a,b, clearly shows that, upon increasing concentration, the most intense adsorption band changes in shape, losing its fine structure, both in water and in acetonitrile solution. This is coupled with a significant drop in molar extinction coefficient on increasing concentration, as shown in Figure 6c,d. As reported in the literature, these findings are consistent with the occurrence of supramolecular aggregation in solution [12, 25].

On the other hand, the longest wavelength band, on increasing concentration, undergoes a redshift, from 441 to 445 nm. As reported in the literature, this suggests the formation of *J*-aggregates [26].

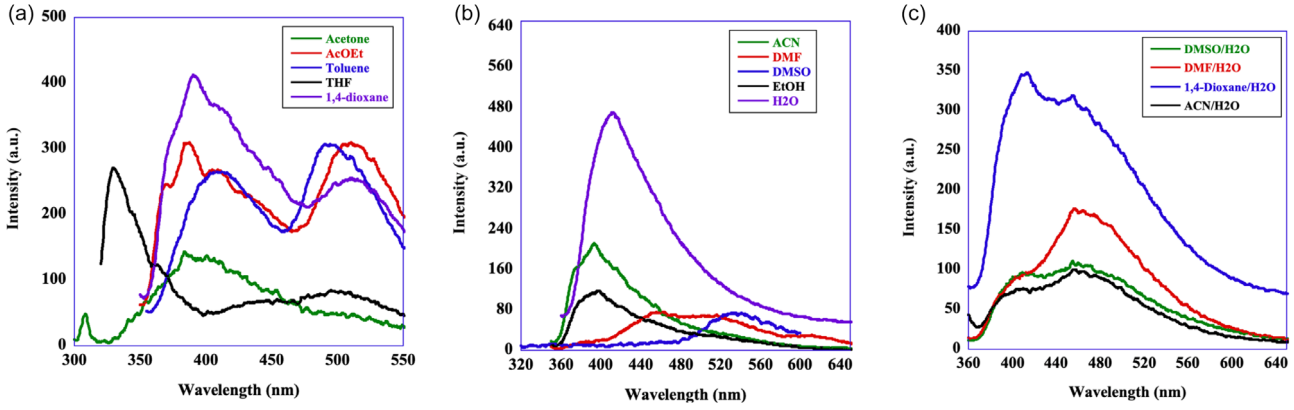

FIGURE 5 | Superimposed Fluorescence spectra of **L-Phe-NI** ($2.8 \cdot 10^{-6}$ M) in (a) apolar aprotic solvents, (b) polar solvents, and (c) binary aqueous solvent mixtures.

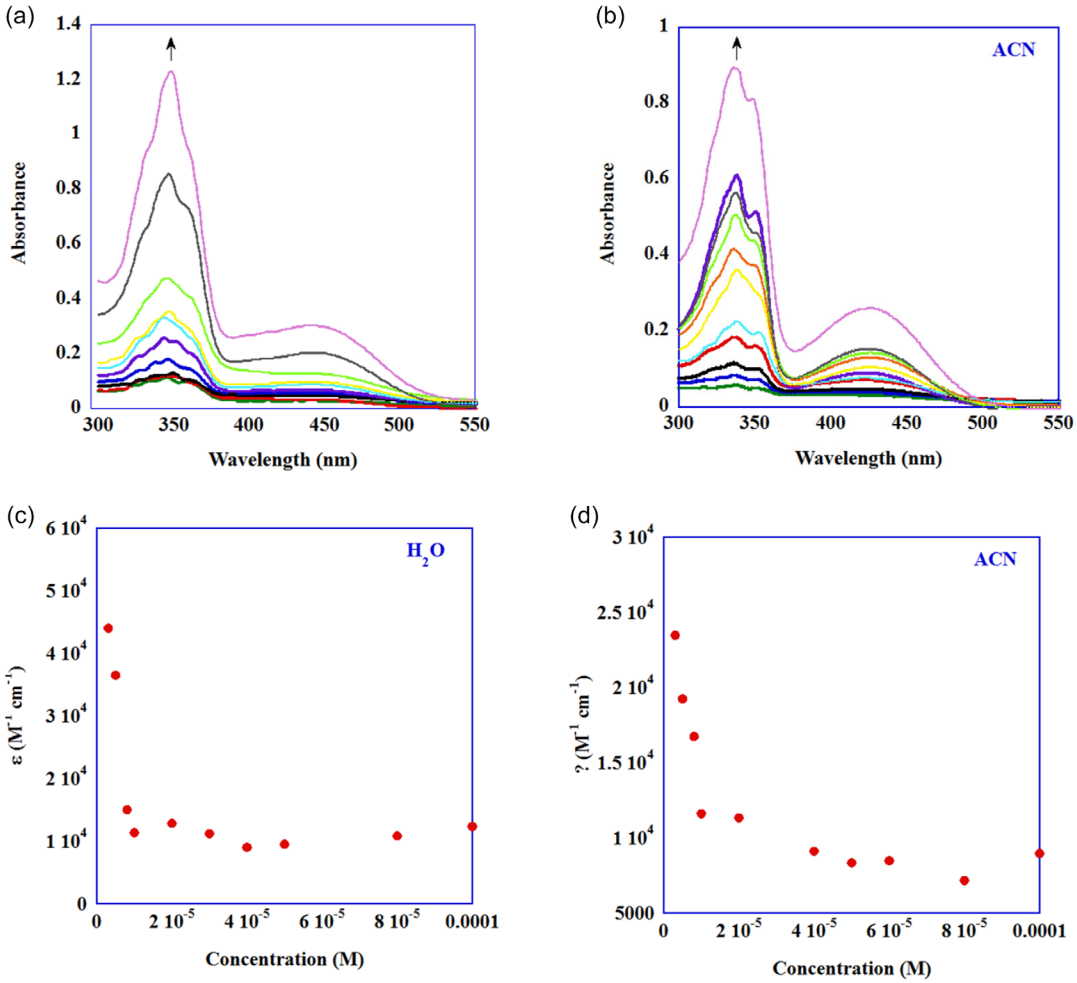

FIGURE 6 | Concentration-dependent UV–vis spectra of **L-Phe-NI** ($3.0 \cdot 10^{-6}$ M ÷ $1.0 \cdot 10^{-4}$ M) in solution of (a) water, (b) acetonitrile; plots of molar extinction coefficients as a function of concentration in (c) water and (d) acetonitrile.

Regarding the spectra of **L-Ala-NI**, as shown in Figure S3a,b, a loss in fine structure of the adsorption band is once again observed on increasing concentration, associated with a small bathochromic shift of 3 nm, with changes in molar extinction coefficients, reported in Figure S3c,d, which are less pronounced compared to the ones of **L-Phe-NI**. Thus, for **L-Ala-NI**, it is more difficult to infer a clear-cut assignment of aggregates to *H*- or *J*-type.

To gain insight into the mechanism of aggregation and the stability of the aggregates, we conducted fluorescence spectra at variable concentrations, for both fluorophores in H_2O and ACN, obtaining the spectra reported in Figure S4. Looking at these spectra shows that for **L-Phe-NI** in water, a loss in fine structure occurs upon increasing the concentration (Figure S4a), while no obvious change in the shape of the spectra is observed in ACN solution (Figure S4b). Similar considerations can be made for **L-Ala-NI**, whose spectra maintain the same shape on increasing concentration. In all cases, fluorescence intensity at λ_{max} increases in a nonlinear way upon increasing concentration, reaching a plateau value, as reported in Figure S5. All these observations are consistent with the formation of supramolecular aggregates in solution. Hence, from these measurements, we determined the aggregation degree α_{agg}, i.e. the molar fraction of aggregates present in solution (see Supporting Information for calculation details).

The plots of α_{agg} as a function of concentration, obtained for **L-Phe-NI**, are reported in Figure 7a,b.

Perusal of the plots reported in Figure 7a,b shows that the trend of α_{agg} as a function of the concentration of **L-Phe-NI** is consistent with an isodesmic pathway of aggregation [27]. Consequently, the nonlinear fit of the curve, by means of equation S1, based on this model [28], allowed us to determine the equilibrium formation constants, K_{agg}, reported in Table 1.

The values of K_{agg} reported in Table 1 clearly show the similar stability of the aggregates of **L-Phe-NI** in the two solvents, although in acetonitrile, α_{agg} reaches the value of 0.5 at a slightly lower concentration.

In the case of **L-Ala-NI**, the plots of α_{agg} as a function of concentration were not consistent with an isodesmic pathway (Figure S6), with a clear threshold concentration after which α_{agg} steeply increases, suggesting the occurrence of a cooperative self-assembly pathway. Consequently, we fitted the data obtained with the simplest cooperative model, called the modified-isodesmic

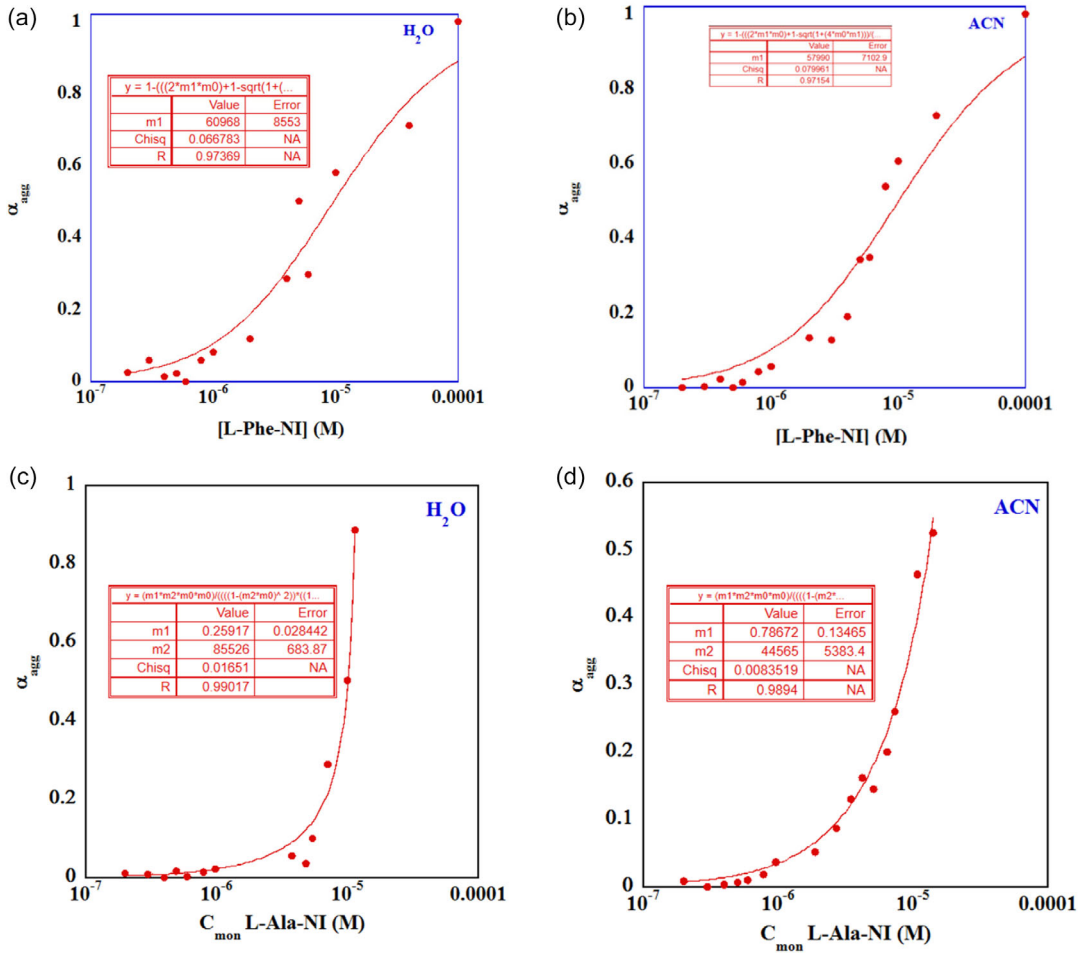

FIGURE 7 | Plots of aggregation degree α_{agg} as a function of concentration for **L-Phe-NI** in solution of (a) water, (b) acetonitrile; plots of α_{agg} as a function of monomer concentration for **L-Ala-NI** in (c) water and (d) acetonitrile.

TABLE 1 | Values of K_{agg} and $C_{\alpha=0.5}$ obtained for **L-Phe-NI**.

Solvent	K_{agg}, M^{-1}	$C_{\alpha=0.5}$, M	*R*
Water	$(6.1 \pm 0.9) \cdot 10^4$	$(5.0 \pm 0.7) \cdot 10^{-6}$	0.97
Acetonitrile	$(5.8 \pm 0.7) \cdot 10^4$	$(8.0 \pm 0.9) \cdot 10^{-6}$	0.97

TABLE 2 | Values of K_{el} and σ obtained for **L-Ala-NI**.

Solvent	K_{el}, M^{-1}	σ	*R*
Water	$(8.6 \pm 0.6) \cdot 10^4$	0.26 ± 0.02	0.99
Acetonitrile	$(4.5 \pm 0.5) \cdot 10^4$	0.8 ± 0.1	0.99

model, in which aggregation occurs with a first equilibrium of dimerization, with constant K_2, and the subsequent elongation steps, all with equilibrium constant K_{el} [29]. According to this model, $K_2 < K_{el}$ and the ratio $\sigma = K_2/K_{el}$ is related to the cooperativity degree, with lower values of σ corresponding to higher cooperativity. Calculation details are reported in the Supporting Information. Fitting of the data according to this model, for **L-Ala-NI**, reported in Figure 7c,d, shows close agreement, and the values of K_{el} and σ are reported in Table 2.

Different from **L-Phe-NI,** for **L-Ala-NI**, the results reported in Table 2 show a clear solvent effect, with aggregation more favorable in water compared with acetonitrile. In particular, in water solution, aggregates are more stable, as evidenced by the higher K_{el} value, but also the degree of cooperativity is higher, as pointed out by the comparison of σ values. This observation can be explained by hydrophobic effects operating in the aqueous solution.

To gain thermodynamic information about the aggregation process of the fluorophores, we carried out temperature-dependent UV–vis measurements recording the spectra of solutions of **L-Phe-NI** and **L-Ala-NI** at concentrations representative of the aggregates, equal to $1.3 \cdot 10^{-4}$ and to $8.0 \cdot 10^{-5}$ M, respectively. The relevant spectra are reported in Figure S7.

Looking at the spectra reported in Figure S7 reveals that, for **L-Phe-NI**, in both solvents, an increase in temperature induces a lowering of the absorbance. On the other hand, for **L-Ala-NI**, absorbance variations in the temperature range considered were too small to be significant, indicating that the temperature range was not sufficiently wide to induce the transition from aggregates to molecularly dissolved species. Consequently, we could determine the thermodynamic parameters only for **L-Phe-NI**. From these spectra, we determined α_{agg} and plotted it as a function of the temperature, obtaining the plots reported in Figure S8a,b. Since, once again, the trend of these plots was consistent with the

TABLE 3 | Thermodynamic parameters and T_m values for **L-Phe-NI**.

Solvent	ΔH_{agg}, kJ/mol	ΔS_{agg}, J K^{-1} mol^{-1}	T_m, °C
Water	−140 ± 8	−370 ± 25	57 ± 0.4
Acetonitrile	−83 ± 4	−200 ± 12	41 ± 0.7

occurrence of an isodesmic aggregation pathway, we calculated the values of K_{agg} at each temperature [29], which were then subjected to a van't Hoff treatment, obtaining the plots reported in Figure S9. Calculation details are reported in Supporting Information, while the values of entropy and enthalpy variations associated with the aggregation process are reported in Table 3.

The thermodynamic parameters obtained are consistent with an enthalpy-driven process of aggregation. In particular, the values of ΔH and ΔS reveal that the aggregates in water are more organized and aggregation is more enthalpically favored. This is also in agreement with the higher value of T_m, i.e. the temperature at which α_{agg} is equal to 0.5, which is also consistent with the higher stability for the aggregates in water, also expressed by the values of K_{agg} in the two solvents. These observations confirm the importance of hydrophobic effects in determining the stability of the aggregates.

2.4 | Morphology of the Aggregates

To investigate the morphology of the supramolecular aggregates formed by both fluorophores, we collected SEM images of samples obtained by solutions of **L-Ala-NI** and **L-Phe-NI** in acetontitrile and water, at concentrations at which they are predominantly present in the aggregated form, equal to $8.0 \cdot 10^{-5}$ and $1.3 \cdot 10^{-4}$ M for **L-Ala-NI** and **L-Phe-NI**, respectively. Since samples were obtained by slow evaporation of solutions of aggregates, we are aware of possible drying effects, altering the actual size of the aggregates as probed by the microscope [30]. Consequently, we herein use SEM images only to gather qualitative information, pertaining only to the morphology of the aggregates and not the size. The SEM images obtained are reported in Figure 8.

Examination of SEM images reported in Figure 8 shows that, in general, aggregates feature the presence of irregularly shaped objects, for which it is difficult to extract a definite morphology, except for **L-Ala-NI** in water, in which elongated objects are further aggregated in flower-like structures.

2.5 | Fluorescence Quantum Yield

To obtain further information on the emissive properties of the fluorophores, we determined their relative emission quantum yields, Φ_F, in the two aggregation-supporting solvents, water and acetonitrile. The emission quantum yields, determined by using 9,10-diphenylanthracene as a standard, are reported in Table 4 and show remarkably high quantum efficiency for **L-Ala-NI** in water, while, once again, the solvent effect is rather marginal for **L-Phe-NI**.

2.6 | Chiral Recognition in Solution

As previously mentioned, supramolecular aggregates can also display chiral recognition ability.

To investigate if the aggregates of **L-Phe-NI** and **L-Ala-NI** show chiral recognition, we probed how the properties of these aggregates change when put in contact with small chiral guest molecules, like those reported in Figure 2. In particular, we studied the effect of these chiral guests on fluorescence emission and RLS spectra. To further investigate the effect of the chirality of the guest molecules, and to ensure that the effects observed are truly deriving from the chirality of the guest molecules and not a generic perturbation of the aggregates, we also employed the enantiomer of **L-Ala-NI**, i.e. **D-Ala-NI**. Since the chiral guest molecules are aromatic alcohols and amines, this investigation was entirely carried out in acetonitrile, due to the insufficient solubility of some of them in water.

The first response to the presence of the chiral guests was the fluorescence emission of the aggregates. To this aim, we prepared solutions of **L-Phe-NI** at the same concentrations representative of the aggregates described previously, adding variable amounts of chiral guests such as (*R*)- and (*S*)-PhEtOH as well as (*R*)- and (*S*)-PhEtNH$_2$. Comparing the effects exerted in the presence of these two chiral guests allows the dissecting of the effect exerted by the number of hydrogen bond donor sites on the chiral discrimination ability. Representative spectra are reported in Figure 9, while the other ones are reported in Figure S10.

The results reported in Figure 9 clearly show that the response of the fluorescent probe **L-Phe-NI** is different in the presence of the single components of both enantiomeric pairs. To better assess the magnitude of chiral recognition, in Figure 10, we report the value of the intensity ratios I_R/I_S, where I_R and I_S are the emissions intensities detected in the presence of the *R*- and *S*- enantiomers of each pair.

Examining the results reported in Figure 10 shows a markedly different response of **L-Phe-NI** in the presence of the two enantiomeric pairs. More specifically, in the presence of enantiomers of PhEtOH, we observed a significant difference in emission only in the presence of 1 eq. of chiral guests. On the other hand, in the presence of PhEtNH$_2$, as reported in Figure 10b, significant differences in emission intensity can be detected already when 0.5 equivalents are present. In addition, the I_R/I_S ratio flips on increasing the amounts of chiral guests to 1 equivalent, as it changes from 0.86 to 1.26. This suggests a stronger interaction of the **L-Phe-NI** aggregates with the hydrogen bond donor group NH$_2$, owing to the higher number of donor sites. Since with PhEtNH$_2$ the highest difference was found in the presence of 0.5 equivalents, we chose this amount to study the response of **L-Ala-NI** on the emission spectra of the aggregates, to the presence of chiral guests, including PhEtOH, PhEtNH$_2$, as well as NaphEtOH and NaphEtNH$_2$, obtaining the results reported in Figure 11.

Differently, to what happens for **L-Phe-NI**, the emission spectra of **L-Ala-NI** are practically unaltered in the presence of enantiomers of PhEtOH, PhEtNH$_2$, and NaphEtOH, while a significant distinction occurs in the case of NaphEtNH$_2$, underlining

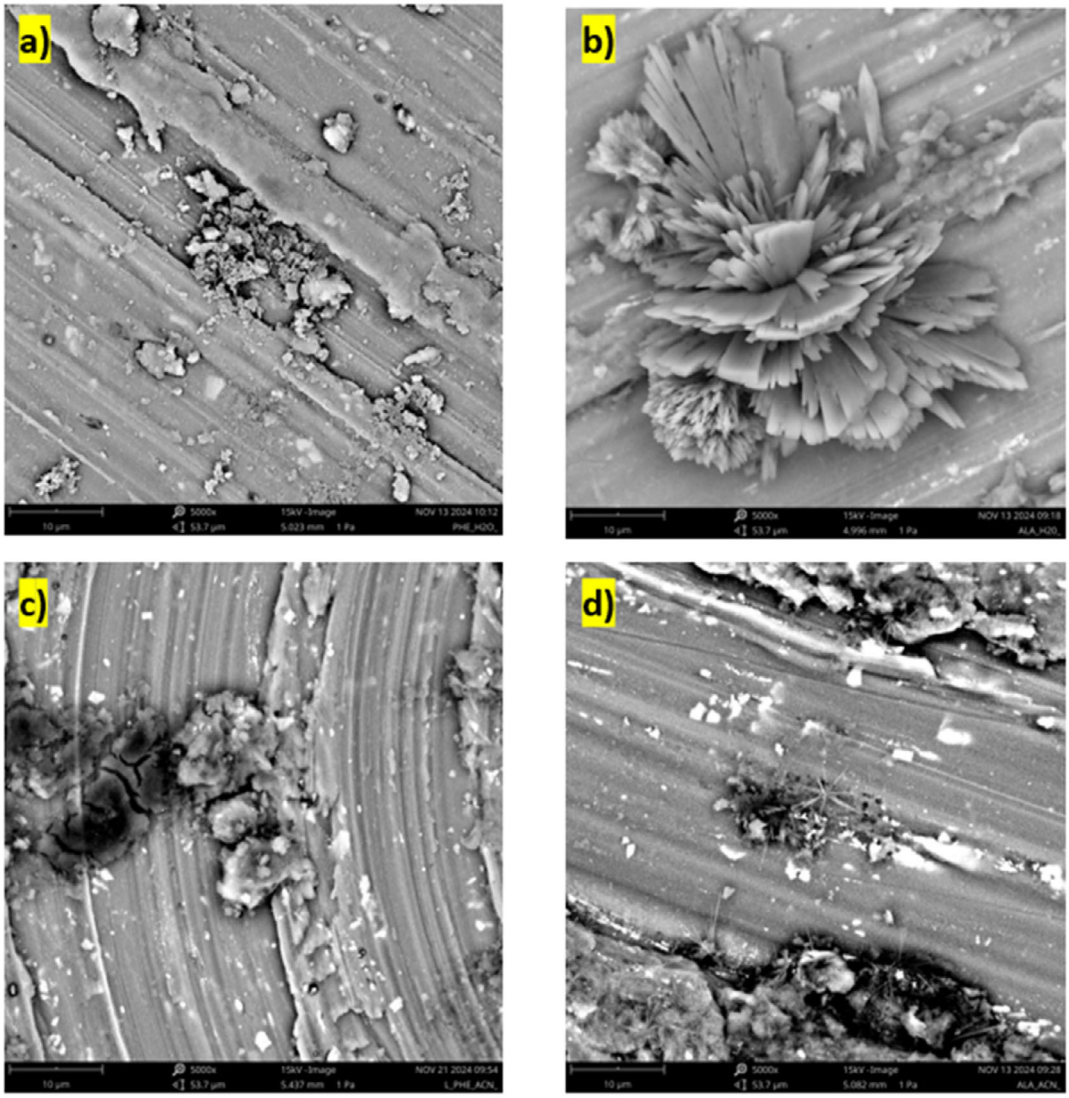

FIGURE 8 | SEM images of aggregates obtained from (a) **L-Phe-NI** in H_2O, (b) **L-Ala-NI** in H_2O, (c) **L-Phe-NI** in ACN, and (d) **L-Ala-NI** in ACN at 5000× magnification level.

TABLE 4 | Relative fluorescence emission quantum yields for **L-Phe-NI** and **L-Ala-NI**.

Solvent	Φ_F L-Phe-NI, %	Φ_F L-Ala-NI, %
Water	3.6	21.0
Acetonitrile	2.2	2.3

that both a higher π-surface area and a higher number of hydrogen bonds are required to elicit sensitivity to the chirality of the guest molecules. This suggests the importance of both hydrogen bonding and π–π interactions in the chiral recognition ability of **L-Ala-NI**. To confirm that the variations observed truly derive from the chirality of the guest molecules and not from a generic perturbation of the aggregates, we conducted the same investigation with the aggregates of **D-Ala-NI**, obtaining the results reported in Figure 11 (red bars).

These results show that in the presence of **D-Ala-NI**, the highest enantiomeric discrimination occurs in the presence of $PhEtNH_2$ and $NaphEtNH_2$, further confirming the importance of both extended π-surface area and a higher number of hydrogen bond donor sites.

To further study the effect of small chiral molecules on the aggregates, and to ascertain the source of variation in the emission spectra of the aggregates, we carried out a similar investigation by RLS measurements. This technique can be useful to investigate supramolecular aggregate systems formed by chromophore-containing molecules [31]. In particular, the intensity of the scattered light can be correlated to the size of aggregates in solution, with higher intensities indicating the occurrence of larger aggregates. As a result, RLS has been employed, for instance, to study a wide range of aggregates, including porphyrins [32], ionic liquids [33] or gels [34] as well as supramolecular aggregates of 1,8-naphthalimide derivatives [13, 35]. Hence, we carried out this investigation to ascertain whether the variation of the emission spectra of the aggregates, as a result of the chirality of the guest molecules, derives from changes in aggregate size. Similarly to the previous approach, we expressed the results in terms of the ratio $I_{RLS\text{-}R}/I_{RLS\text{-}S}$, where

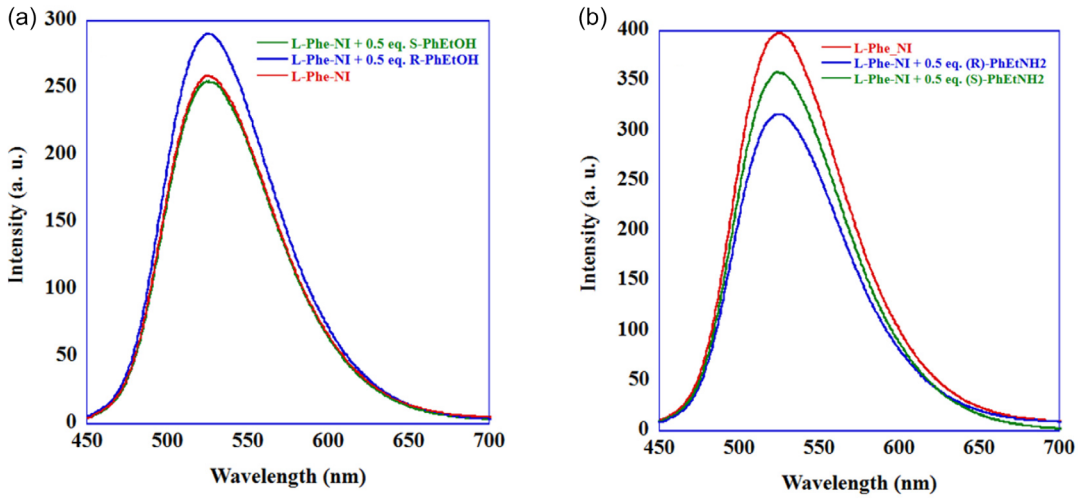

FIGURE 9 | Fluorescence emission spectra of acetonitrile solutions of **L-Phe-NI** ($1.3 \cdot 10^{-4}$ M), in the presence of 0.5 eq. of (a) (*R*)- and (*S*)-PhEtOH and (b) (*R*)- and (*S*)-PhEtNH$_2$.

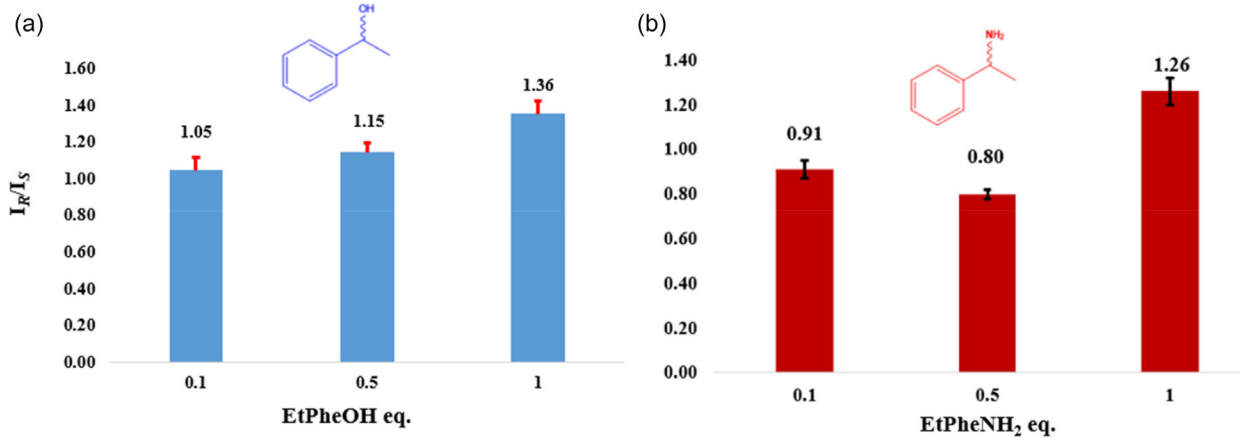

FIGURE 10 | Values of I_R/I_S from fluorescence spectra of acetonitrile solutions of **L-Phe-NI** ($1.3 \cdot 10^{-4}$ M), in the presence of variable amounts of (a) (*R*)- and (*S*)-PhEtOH and (b) (*R*)- and (*S*)-PhEtNH$_2$.

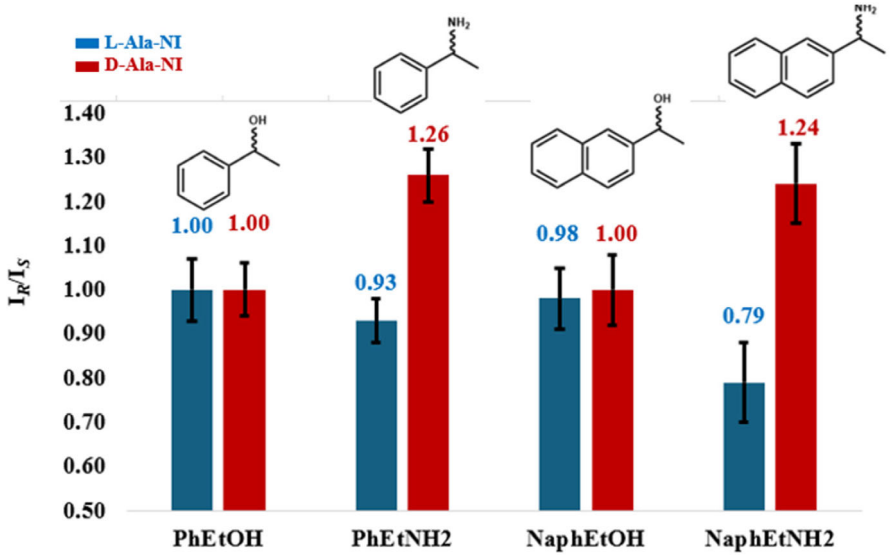

FIGURE 11 | Values of I_R/I_S from fluorescence spectra of acetonitrile solutions of **L-Ala-NI** or **D-Ala-NI** ($8.0 \cdot 10^{-5}$ M), in the presence of 0.5 eq. of (*R*)- and (*S*)-PhEtOH, (*R*)- and (*S*)-PhEtNH$_2$, (*R*)- and (*S*)-NaphEtOH and (*R*)- and (*S*)-NaphEtNH$_2$.

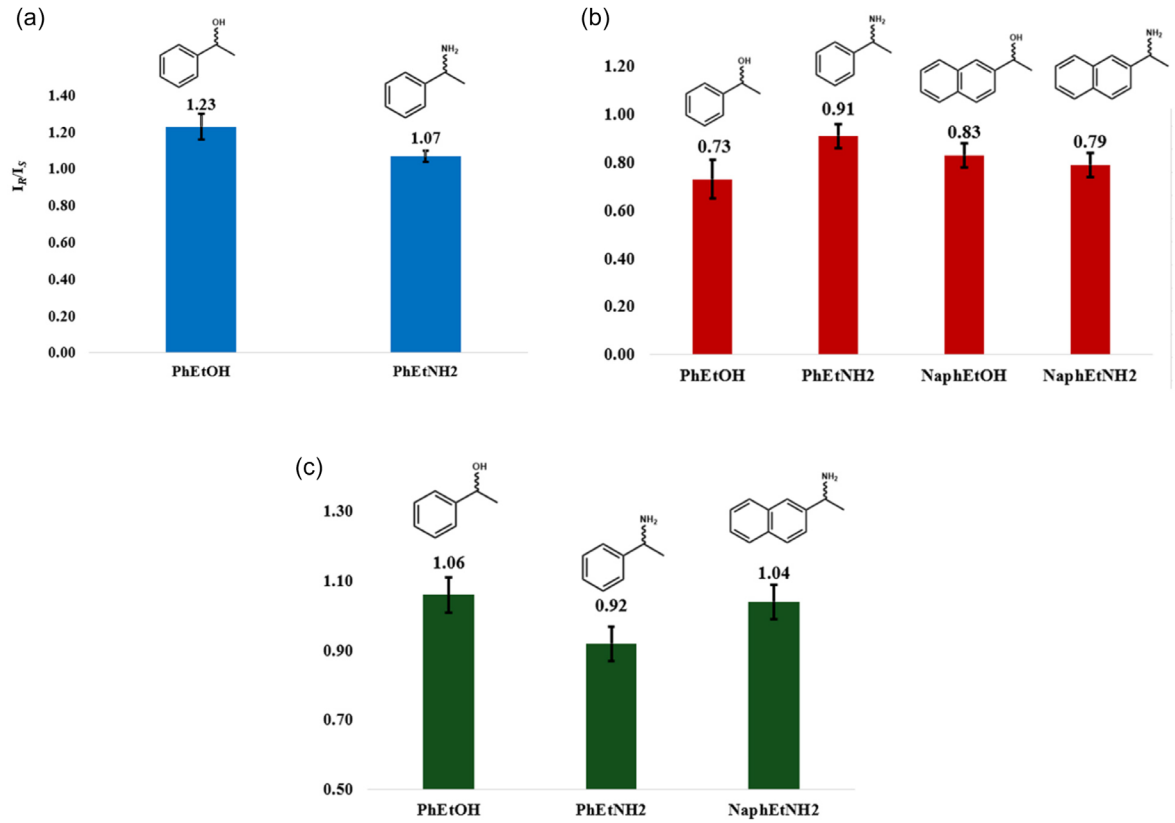

FIGURE 12 | Values of $I_{RLS\text{-}R}/I_{RLS\text{-}S}$ from RLS spectra of acetonitrile solutions of (a) **L-Phe-NI** ($1.3 \cdot 10^{-4}$ M) in the presence of 0.5 eq. of (*R*)- and (*S*)-PhEtOH, (*R*)- and (*S*)-$PhEtNH_2$ (b) **L-Ala-NI** ($8.0 \cdot 10^{-5}$ M) in the presence of 0.5 eq. of (*R*)- and (*S*)-PhEtOH, (*R*)- and (*S*)-$PhEtNH_2$, (*R*)- and (*S*)-NaphEtOH and (*R*)- and (*S*)-$NaphEtNH_2$, and (c) **D-Ala-NI** ($8.0 \cdot 10^{-5}$ M) in the presence of 0.5 eq. of (*R*)- and (*S*)-PhEtOH, (*R*)- and (*S*)-$PhEtNH_2$ and (*R*)- and (*S*)-$NaphEtNH_2$.

$I_{RLS\text{-}R}$ and $I_{RLS\text{-}R}$ are the RLS intensities detected in the presence of the *R*- and *S*-enantiomers of the chiral pair, respectively. The results obtained for **L-Phe-NI** and **L-Ala-NI**, in the presence of 0.5 eq. of guest molecules, are reported in Figure 12a,b, while the relevant RLS spectra are reported in Figures S12, 13.

The results reported in Figure 12a show that, in general, for **L-Phe-NI**, the presence of chiral molecules PhEtOH and $PhEtNH_2$ induces an increase in the size of the aggregates as evidenced by the increase of I_{RLS} in both cases. However, the ratios $I_{RLS\text{-}R}/I_{RLS\text{-}S}$, reported in Figure 12a, appear unrelated to the trend of I_R/I_S found from the fluorescence spectra, given that no chiral discrimination occurs in the presence of $PhEtNH_2$. Similar considerations can be made for **L-Ala-NI**, as, once again, addition of chiral molecules results in a slight increase of I_{RLS} (Figure S14). Notably, as shown in Figure 12b, the $I_{RLS\text{-}R}/I_{RLS\text{-}S}$ are in most cases significantly different from unity, although they follow an articulate trend as a function of the structure of the enantiomeric pairs. In particular, while for the fluorescence spectra the most marked enantiomeric discrimination occurred in the presence of $NaphEtNH_2$, for RLS spectra, the magnitude of the $I_{RLS\text{-}R}/I_{RLS\text{-}S}$ ratios, although different than unity, is similar for all the enantiomeric pairs considered. This suggests that, although interaction with chiral molecules does affect the size of the aggregates, this phenomenon is not directly correlated to the changes in emission spectra observed. Finally, considering the effect exerted on the RLS spectra by the same enantiomeric pairs on the aggregates of **D-Ala-NI**, shown in Figures S14 and 12c, the $I_{RLS\text{-}R}/I_{RLS\text{-}S}$ ratios flip in values, compared with **L-Ala-NI,** suggesting a true effect of chirality on the size of the aggregates, although their magnitude is in any case close to unity, further supporting the marginal effect of the changes in aggregates size on the emission spectra.

2.7 | ^{1}H-NMR Investigation

The results so far obtained have evidenced the possibility of chiral discrimination, particularly in the case of **L-Ala-NI**. Consequently, to gain information about the interaction mode between the fluorophores and the chiral guest, we carried out a ^{1}H-NMR investigation by recording the chemical shift variation upon interaction of our fluorophores with the chiral guests. In particular, we chose *R*- and *S*-$PhEtNH_2$. The spectra, obtained in D_6-DMSO, in the presence of 0.5 eq. of *R*- or *S*-$PhEtNH_2$, are reported in Figure S15, while the values of chemical shift variations are reported in Table 5.

Perusal of the results reported in Table 5 clearly shows that the presence of *R*- or *S*-$PhEtNH_2$ does not affect the position of the signal of the aromatic protons of **L-Ala-NI**. Conversely, the most significant chemical shift variations involve the aliphatic C–H of the fluorophore, at 5.58 ppm (proton F in Figure S15), which moves upfield by 0.25 ppm in the presence of each enantiomer of $PhEtNH_2$. This suggests the inclusion of this group in the shielding cone generated by the phenyl ring of the amine. As

TABLE 5 | ^{1}H-NMR chemical shifts and chemical shift variations of **L-Ala-NI**, $PhEtNH_2$, and mixtures of **L-Ala-NI** with 1 eq. of (*R*)- and (*S*)-$PhEtNH_2$.

δ $PhEtNH_2$, ppm	δ L-Ala-NI, ppm	δ L-Ala-NI + (*R*)-$PhEtNH_2$, ppm	δ L-Ala-NI + (*S*)-$PhEtNH_2$, ppm	$\Delta\delta$ *R*, ppm	$\Delta\delta$ *S*, ppm
	8.51	8.51	8.52	0	0.01
	8.39	8.36	8.37	−0.03	−0.02
	7.98	7.99	7.98	0.01	—
7.34		7.42	7.43	0.08	0.09
	5.58	**5.34**	**5.37**	**−0.24**	**−0.21**
3.96		**4.25**	**4.26**	**0.29**	**0.3**
	1.55	1.51	1.53	−0.04	−0.02
1.24		**1.43**	**1.45**	**0.19**	**0.21**

far as the protons of *R*- or *S*-$PhEtNH_2$ are concerned, the largest chemical shift variations involve the aliphatic C–H at 3.96 ppm and the methyl group in the side chain at 1.24 ppm (protons 4 and 5 in Figure S16), which move downfield by 0.3 ppm. A smaller but consistent downfield shift can also be observed for the aromatic protons of *R*- or *S*-$PhEtNH_2$, which rules out the occurrence of face-to-face π-stacking interactions. The whole of these findings suggest that **L-Ala-NI** interacts with *R*- or *S*-$PhEtNH_2$ adopting the arrangement depicted in Figure S16, allowing the establishment of slipped-stacking π–π interactions, which is similar to what has been reported in the literature for related substrates [13].

It is however, important to note, as a caveat, that the NMR spectrum was recorded in DMSO, instead of acetonitrile, for solubility reasons. Therefore, the arrangement proposed in Figure S16 should be considered as a plausible interaction model rather than a definitive binding mode.

Finally, based on the evidence mentioned above, and in agreement with a previous study on supramolecular aggregates of functionalized 1,8-naphthalimides [13], we propose a simplified scheme for the recognition mechanism, reported in Figure 13.

In such a hypothesis, the interaction of the chiral guest molecules by π–π interactions with the **L-Ala-NI** or **L-Phe-NI** determines a perturbation and a partial disassembly of the aggregates. The chiral nature of these latter induces a different magnitude of interaction and extent of disassembly, leading to a different fluorescence response.

2.8 | Incorporation of the Fluorophore Onto Solid Supports: Filter Paper Strips and PHB Polymer Film

After having ascertained the possibility of chiral recognition by **L-Ala-NI** in solution, we went on to investigate whether this property is maintained when the fluorophore is incorporated into solid supports, such as filter paper strips and poly(3-hydroxybutirate) (PHB) films. For the incorporation of **L-Ala-NI** in filter paper strips, we soaked three filter square strips (2 cm × 2 cm) into a solution of **L-Ala-NI** in chloroform ($8.0 \cdot 10^{-5}$ M). Chloroform was chosen to facilitate room temperature drying. Subsequently, after being dried, two of these strips were further soaked in a hexane solution ($4.0 \cdot 10^{-5}$ M) of (*R*)- or (*S*)-$PheEtNH_2$. Finally, we recorded the solid-state spectra of the three strips to evaluate if the chiral recognition ability of **L-Ala-NI** is maintained. The spectra obtained are reported in Figure 14a.

As a blank control, we recorded the fluorescence spectrum of the pristine paper strip, treated in the same way, but put in contact only with the neat solvents, observing negligible emission compared with the paper strip in which **L-Ala-NI** was embedded

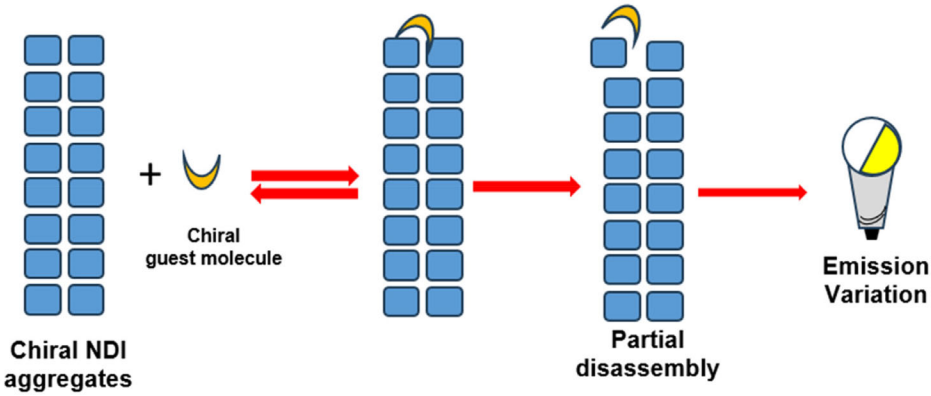

FIGURE 13 | Schematic simplified representation of the possible recognition mechanism by chiral aggregates of **L-Ala-NI** or **L-Phe-NI**, with chiral guest molecules.

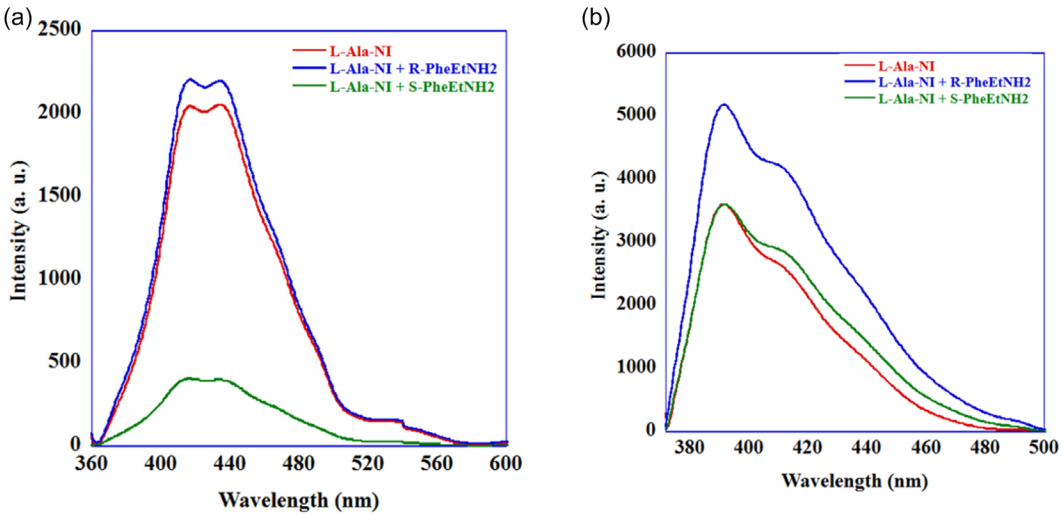

FIGURE 14 | Solid-state Fluorescence emission **L-Ala-NI** and **L-Ala-NI** with (*R*)- and (*S*)-PhEtNH$_2$, embedded onto (a) filter paper strips and (b) PHB films.

(Figure S17). The spectra reported in Figure 14a show a clear distinction between the spectra of **L-Ala-NI** in the presence of each enantiomer of PhEtNH$_2$; more specifically, the presence of (*R*)-PhEtNH$_2$ does not significantly affect the emission intensity of the fluorophore in the paper strip, while, on the other hand, a marked quenching occurs in the presence of (*S*)-PhEtNH$_2$. Based on duplicate experiments, the value of I_R /I_S in this case is (5.5 ± 0.2), which is much higher than the one obtained in solution, evidencing that incorporation of the fluorophore onto a solid support not only maintains but enhances its chiral recognition ability.

Encouraged by the results obtained in the filter paper strips, we employed a similar approach to incorporate the same fluorophore onto PHB polymer films. The film containing **L-Ala-NI** was prepared by solvent casting from a solution obtained by dissolving PHB in a chloroform solution ($8.0 \cdot 10^{-5}$ M) of **L-Ala-NI**. Following the same approach employed for the filter paper strips, we then took square sections of these films and immersed them for 10 min in hexane solutions ($4.0 \cdot 10^{-5}$ M) of (*R*)- or (*S*)-PheEtNH$_2$. Representative pictures of these films are reported in Figure S18. After drying, we recorded the emission spectra of the films, obtaining the results reported in Figure 12b. As a blank control, no significant emission was displayed by the pristine polymer film under the conditions used. The spectra reported in Figure 14b show, once again, that chiral recognition is maintained. Notably, the emission behavior appears opposite to that found for the paper strips, given that in this case, it is the (*S*)-PhEtNH$_2$ which does not affect the emission of the fluorophore, while (*R*)-PhEtNH$_2$ induces an emission enhancement. In this case, the value of I_R/I_S is (1.4 ± 0.2), which is lower than the one detected in the paper strips, but close to the one observed in solution. The whole of these results highlights the promising potential of such fluorophores to be employed in solid-state devices for chiral recognition. The different behavior of the aggregates of **L-Ala-NI**, as already viewed, can be ascribed to a different local microenvironment in which the fluorescent probe is embedded. This sensitivity of the emission of fluorophores has already been reported in the literature for π-conjugated molecules, and has been linked to local packing effects or microheterogeneity of the polymer matrix [36, 37].

3 | Conclusions

In this work, we prepared three amino acid-functionalized 1,8-naphthalimides, namely **L-Phe-NI**, **L-Ala-NI**, and **D-Ala-NI**. We studied the photophysical properties of the fluorophores, finding that they assemble into *J*-type aggregates in acetonitrile and water solutions. Concentration- and temperature-dependent UV–vis and fluorescence spectroscopy measurements revealed that **L-Phe-NI** self-assembles following an isodesmic pathway, whereas aggregation of **L-Ala-NI** occurs via a cooperative mechanism. Then, we studied the chiral recognition ability of the fluorophores toward the components of enantiomeric pairs of aromatic alcohols and amines, differing in the π-surface area extension, namely (*R*)- and (*S*)-1-phenylethanol (PhEtOH), (*R*)- and (*S*)-1-phenetylethylamine (PhEtNH$_2$), (*R*)- and (*S*)-1-(2-naphthyl)-ethanol (NaphEtOH) and (*R*)- and (*S*)-1-(2-naphthyl)-ethylamine (NaphEtNH$_2$), by fluorescence measurements. We found that the best probe in terms of chiral recognition was **L-Ala-NI**, while comparison with the enantiomeric probe **D-Ala-NI** confirmed that the differences in fluorescence intensity emission derived truly from the chirality of the molecules and not from a generic perturbation of the aggregates. RLS measurements point out that the chiral guest molecules affected the size of the aggregates, but exerted a marginal role in the recognition process, while ^{1}H-NMR investigation suggested that the chiral guest molecules interact with the aggregates of **L-Ala-NI**, adopting a slipped-stacked arrangement. Finally, we verified that the aggregates of **L-Ala-NI** maintain their chiral recognition ability also when embedded onto solid supports like PHB polymer films and filter paper strips. In this latter case, the emission intensity ratio I_R/I_S was even higher than the one detected in solution; notably, changing the nature of the solid support changed the selectivity of the probe toward each enantiomer of PhEtNH$_2$.

4 | Experimental Section

4.1 | Materials

4-chloro-1,8-naphthalic anhydride, L-phenylalanine, D-alanine, L-alanine, (*R*)-1-phenylethanol, (*S*)-1-phenylethanol, (*R*)-1-phenylethylamine, (*S*)-1-phenylethylamine, (*R*)-1-(2-naphthyl)-ethanol, (*S*)-1-(2-naphthyl)-ethanol, (*R*)-1-(2-naphthyl)-ethylamine, (*S*)-1-(2-naphthyl)-ethylamine, poly(3-hydroxybutirate), 9,10-diphenylanthracene, triethylamine and hydrochloric acid (37% w:w), were obtained from commercial sources and used without further purification. Spectroscopic grade toluene, dichloromethane, dimethylformamide, acetonitrile, ethanol, acetone, chloroform, and ethyl acetate were purchased and used without further purification.

4.2 | Synthesis of Fluorophores

The synthesis of fluorophores was carried out by following a previously reported procedure [22].

4-chloro-1,8-napthalic anhydride (0.5 g, $2.14 \cdot 10^{-3}$ mol) was suspended in 20 mL of DMF and added with the stoichiometric amount of amino acid and 0.1 mL of triethylamine. The resulting mixture was kept at 90°C under stirring for 12 h. Subsequently, the reaction mixture was allowed to cool down at room temperature, followed by the addition of 50 mL of HCl 3 M, inducing the precipitation of a yellow-orange solid. The precipitate was filtered off and washed with deionized water.

4.3 | L-Phe-NI

Orange-yellow solid; Yield: 87%; m.p. 201–105°C; ^{1}H-NMR (300 MHz, DMSO-d_6) δ: 2.51 (m, 1H), 5.87 (m, 1H), 7.09 (m, 5H), 7.99 (dd, $J_1 = 12.0$ Hz, $J_2 = 6.0$ Hz, 2H), 8.40 (d, $J = 6.0$ Hz, 1H), 8.56 (dd, $J_1 = 12.0$ Hz, $J_2 = 6.0$ Hz, 2H) ppm; ^{13}C-NMR (300 MHz, DMSO-d_6) δ: 34.6, 54.5, 121.0, 122.3, 126.8, 128.4, 128.6, 128.9, 129.2, 129.4, 131.1, 131.9, 132.7, 138.2, 138.6, 162.7, 163.0, 171.0 ppm.

4.4 | L-Ala-NI

Pale yellow solid. Yield: 77%; m.p. > 250°C. ^{1}H-NMR (400 MHz, DMSO-d_6) δ: 1.55 (d, $J = 7.0$ Hz, 3H), 5.58 (m, 1H), 7.98 (m, 2H), 8.39 (d, $J = 8.0$ Hz, 1H), 8.51 (m, 2H), 12.73 (s, 1H) ppm. ^{13}C-NMR (400 MHz, DMSO-d_6) δ: 14.9, 49.1, 121.5, 122.9, 128.2, 128.7, 128.8, 129.1, 130.8, 131.7, 132.4, 138.3, 162.9, 162.6, 171.7 ppm.

4.5 | D-Ala-NI

Pale yellow solid: Yield: 69%; m.p. > 250°C. ^{1}H-NMR (400 MHz, DMSO-d_6) δ: 1.55 (d, $J = 7.0$ Hz, 3H), 5.56 (m, 1H), 7.98 (m, 2H), 8.39 (d, $J = 8.0$ Hz, 1H), 8.54 (m, 2H), 12.73 (s, 1H) ppm.

4.6 | UV–Vis and Fluorescence Spectroscopy Measurements

Samples for UV–vis and fluorescence spectroscopy were prepared by dilution of stock solutions in chloroform. The suitable volume of solution was transferred to a vial, and the solvent was evaporated at reduced pressure. Then, the residue was dissolved in 2 mL of the appropriate solvent. All the solutions were limpid after this treatment. UV–vis spectra were recorded at 25°C on a Beckmann DU800 spectrophotometer equipped with a Peltier temperature controller, employing quartz cuvettes with 1 cm optical path.

Samples for fluorescence spectroscopy were degassed prior to measurement. Spectra were recorded with a JASCO spectrofluorometer using quartz cuvettes with 0.2 cm optical path, and λ_{exc} was set at the maximum absorbance wavelength, while excitation and emission bandwidths were set at 3 nm. Relative fluorescence quantum yields were determined by a reported procedure [38]. Quantum yields were determined at 25°C, relative to 9,10-diphenylanthracene in ethanol or sodium fluorescein in NaOH 0.1 M, employing the standard quantum yield values reported in the literature [39]. RLS measurements were carried out using a synchronous scanning mode in which the excitation and emission monochromators were set at the same wavelength. The RLS spectra were recorded from 290 to 750 nm with both the excitation and emission slit widths set at 3.0 nm. Samples were prepared as described above. Measurements were carried out in triplicate.

4.7 | Solid State Fluorescence Spectra

Solid-state fluorescence spectra were recorded from films obtained by casting 200 µL of water or acetonitrile solution of the fluorophores, at concentrations representative of the aggregates. The solvent was removed by evaporation at room temperature, obtaining a solid thin film. To ensure a meaningful comparison between solid- and solution-phase spectra, the excitation spectra were recorded for each sample. Emission spectra were obtained by exciting the samples at the λ_{max} obtained from the excitation spectra.

4.8 | Chiral Recognition

Chiral recognition experiments were carried out following a procedure reported in the literature [5].

Samples for typical measurements were prepared by adding suitable amounts of chiral molecules to a solution containing a fixed concentration of fluorophore, at a concentration of $1.0 \cdot 10^{-4}$ M.

Each sample was then heated at 40°C for 2 min, then allowed to cool at room temperature for 30 min, prior to measurements. Fluorescence emission spectra were obtained as described above. Each measurement was carried out in triplicate.

Chiral recognition experiments on paper strips were carried out by soaking for 10 min, three square paper strips (2 cm × 2 cm) in an $8.0 \cdot 10^{-5}$ M chloroform solution of **L-Ala-NI**. The stripes were dried at room temperature for 24 h. Subsequently, the emission

spectra of each strip were obtained by irradiating the sample at the λ_{max} obtained in the previously recorded excitation spectrum (348 nm).

Two strips were immersed in $4 \cdot 10^{-5}$ M hexane solutions of (*R*)- or (*S*)- 1-phenylethylamine for 10 min and left to dry at room temperature. Finally, the fluorescence emission spectra of these strips were recorded as described above.

PHB films were prepared by dissolving 0.5 g of PHB in 12 mL of chloroform at 50°C, to which 5 mL of a solution of **L-Ala-NI** $8.0 \cdot 10^{-5}$ M in chloroform was added. The resulting solution was then transferred to a Petri dish and left to dry overnight at room temperature. Subsequently, square sections of the film, 2 cm × 2 cm, were soaked for 10 min in hexane solutions ($4.0 \cdot 10^{-5}$ M) of (*R*)- and (*S*)-PhEtNH$_2$ and left to dry at room temperature. Emission spectra were recorded as previously described.

Acknowledgments

We thank University of Palermo (FFR 2025) for funding.

Open access publishing facilitated by Universita degli Studi di Palermo, as part of the Wiley - CRUI-CARE agreement.

Conflicts of Interest

The authors declare no conflicts of interest.

Data Availability Statement

The data that supports the findings of this study are available in the supplementary material of this article.

References

1. Y. Yang, L. Liu, and Z. Wei, "Chiral Conjugated Molecular Assemblies Interact with Substances and Light," *Accounts of Materials Research* 5 (2024): 329–346.

2. A. R. A. Palmans and E. W. Meijer, "Amplification of Chirality in Dynamic Supramolecular Aggregates," *Angewandte Chemie, International Edition* 46 (2007): 8948–8968.

3. Y. Wang, J. Xu, Y. Wang, and H. Chen, "Emerging Chirality in Nanoscience," *Chemical Society Reviews* 42 (2013): 2930–2962.

4. Y. Li, K. Yu, Z. Xu, et al., "Rapid Enantioselective Fluorescence Recognition and Chiral Separation of Free Amino Acids," *Nature Communications* 17 (2026): 96.

5. R. Randazzo, M. Gaeta, C. M. A. Gangemi, M. E. Fragalà, R. Purrello, and A. D'Urso, "Chiral Recognition of L- and D- Amino Acid by Porphyrin Supramolecular Aggregates," *Molecules* 24 (2018): 84–84.

6. T. L. G. Cabral, J. P. B. Da Silva, C. F. Tormena, and M. Stein, "Molecular Recognition and Chiral Discrimination from NMR and Multi-Scale Simulations," *Chemistry – A European Journal* 31 (2025): e202404694.

7. C. Aroulanda and P. Lesot, "Molecular Enantiodiscrimination by NMR Spectroscopy in Chiral Oriented Systems: Concept, Tools, and Applications," *Chirality* 34 (2022): 182–244.

8. Y. Okamoto and T. Ikai, "Chiral HPLC for Efficient Resolution of Enantiomers," *Chemical Society Reviews* 37 (2008): 2593.

9. F. Feizi, M. Shamsipur, M.-B. Gholivand, et al., "Fluorescence and Circular Dichroism Dual-Mode Probe for Chiral Recognition of Tyrosine and Its Applications in Bioimaging," *Acs Applied Materials & Interfaces* 16 (2024): 48058–48072.

10. L. Pu, "Fluorescence of Organic Molecules in Chiral Recognition," *Chemical Reviews* 104 (2004): 1687–1716.

11. G. Zhang, X. Cheng, Y. Wang, and W. Zhang, "Supramolecular Chiral Polymeric Aggregates: Construction and Applications," *Aggregate* 4 (2023): e262.

12. S. Marullo, E. Capuano, and F. D'Anna, "Supramolecular Aggregates from Core-Functionalized 1,8-Naphthalimides: Insights into Self-Assembling and Sensing Ability for Drugs in Water," *Dyes and Pigments* 241 (2025): 112881–112881.

13. S. Marullo, R. Arena, G. Lazzara, G. Cavallaro, M. Cacioppo, and F. D'Anna, "Fast and Efficient Sensing of Drugs in Water Using Self-Assembling D-Glucamine-Functionalized Naphthalenediimide and 1,8-Naphthalimide Fluorophores," *Chemistry – A European Journal* 30 (2024): e202401944.

14. X. Chen, N. Hu, H. Wei, and H. Wang, "Chiral Fluorescent Recognition by Naphthalimide," *Journal of Fluorescence* 30 (2020): 679–685.

15. Y. D. Karmakar, P. Khanra, B. Ghosh, L. Roy, and A. Das, "Circularly Polarized Luminescence (CPL)-Active Homo- and Heterostructures by Surface-Catalyzed Secondary Supramolecular Polymerization," *Small* 22 (2026): e12262.

16. S. Liu, F. Li, Y. Wang, X. Li, C. Zhu, and Y. Cheng, "Circularly Polarized Luminescence of Chiral 1,8-Naphthalimide-Based Pyrene Fluorophore Induced via Supramolecular Self-Assembly," *Journal of Materials Chemistry C* 5 (2017): 6030–6036.

17. S. Kuila, S. Misra, T. Singha, et al., "Pathway Complexity of Kinetically Trapped Dipeptide-Based Metastable State: Supramolecular Structural Transformation and Helicity Tuning," *Small* 21 (2025): 2501718.

18. H. Hu, Q. Yuan, J. Xie, et al., "Naphthalimide-Based π-Conjugated Chiral Foldamers: Cascade-Integrated Construction Strategy, Structural Analysis and Chiroptical Properties," *Science China Chemistry* 69 (2026): 833–843.

19. H.-Q. Dong, T.-B. Wei, X.-Q. Ma, et al., "1,8-Naphthalimide-Based Fluorescent Chemosensors: Recent Advances and Perspectives," *Journal of Materials Chemistry C* 8 (2020): 13501–13529.

20. M. S. Alexiou, V. Tychopoulos, S. Ghorbanian, J. H. P. Tyman, R. G. Brown, and P. I. Brittain, "The UV–Visible Absorption and Fluorescence of Some Substituted 1,8-Naphthalimides and Naphthalic Anhydrides," *Journal of the Chemical Society, Perkin Transactions* 2 (1990): 837–842.

21. T. Anand, S. K. A. Kumar, and S. K. Sahoo, "A New Al3+ Selective Fluorescent Turn-on Sensor Based on Hydrazide-Naphthalic Anhydride Conjugate and Its Application in Live Cells Imaging," *Spectrochimica Acta, Part A: Molecular and Biomolecular Spectroscopy* 204 (2018): 105–112.

22. M. Pandeeswar, H. Khare, S. Ramakumar, and T. Govindaraju, "Crystallographic Insight-Guided Nanoarchitectonics and Conductivity Modulation of an n-Type Organic Semiconductor Through Peptide Conjugation," *Chemical Communications* 51 (2015): 8315–8318.

23. R. Greiner, T. Schlücker, D. Zgela, and H. Langhals, "Fluorescent Aryl Naphthalene Dicarboximides with Large Stokes Shifts and Strong Solvatochromism Controlled by Dynamics and Molecular Geometry," *Journal of Materials Chemistry C* 4 (2016): 11244–11252.

24. C. Felip-León, F. Galindo, and J. F. Miravet, "Insights into the Aggregation-Induced Emission of 1,8-Naphthalimide-Based Supramolecular Hydrogels," *Nanoscale* 10 (2018): 17060–17069.

25. R. J. Das and K. Mahata, "Mutualistic Benefit in the Self-Sorted Co-Aggregates of *Peri* -Naphthoindigo and a 4-Amino-1,8-Naphthalimide Derivative," *Soft Matter* 15 (2019): 5282–5286.

26. A. Eisfeld and J. S. Briggs, "The J- and H-Bands of Organic Dye Aggregates," *Chemical Physics* 324 (2006): 376–384.

27. B. Heyne, "Self-Assembly of Organic Dyes in Supramolecular Aggregates," *Photochemical & Photobiological Sciences* 15 (2016): 1103–1114.

28. Z. Chen, A. Lohr, C. R. Saha-Möller, and F. Würthner, "Self-Assembled π-Stacks of Functional Dyes in Solution: Structural and Thermodynamic Features," *Chemical Society Reviews* 38 (2009): 564–584.

29. M. M. J. Smulders, M. M. L. Nieuwenhuizen, T. F. A. de Greef, P. van der Schoot, A. P. H. J. Schenning, and E. W. Meijer, "How to Distinguish Isodesmic from Cooperative Supramolecular Polymerisation," *Chemistry – A European Journal* 16 (2010): 362–367.

30. B. Michen, C. Geers, D. Vanhecke, et al., "Avoiding Drying-Artifacts in Transmission Electron Microscopy: Characterizing the Size and Colloidal State of Nanoparticles," *Scientific Reports* 5 (2015): 9793.

31. P. J. Collings, E. J. Gibbs, T. E. Starr, et al., "Resonance Light Scattering and Its Application in Determining the Size, Shape, and Aggregation Number for Supramolecular Assemblies of Chromophores," *Journal of Physical Chemistry B* 103 (1999): 8474–8481.

32. J. C. De Paula, J. H. Robblee, and R. F. Pasternack, "Aggregation of Chlorophyll a Probed by Resonance Light Scattering Spectroscopy," *Biophysical Journal* 68 (1995): 335–341.

33. F. D'Anna, F. Ferrante, and R. Noto, "Geminal Ionic Liquids: A Combined Approach to Investigate Their Three-Dimensional Organisation," *Chemistry – A European Journal* 15 (2009): 13059–13068.

34. F. Billeci, M. Buttacavoli, E. Peri, S. Marullo, P. Cancemi, and F. D'Anna, "Unravelling the Properties of Fluorescent Ammonium Salts to Obtain Thixotropic Hydrogels with Antitumoral Activity," *ACS Omega* 11 (2026): 663–680.

35. C. Rizzo, P. Cancemi, L. Mattiello, S. Marullo, and F. D'Anna, "Naphthalimide Imidazolium-Based Supramolecular Hydrogels as Bioimaging and Theranostic Soft Materials," *ACS Applied Materials & Interfaces* 12 (2020): 48442–48457.

36. T. Matsushita, T. Tanaka, Y. Sawatari, and G. Konishi, "Fluorescence Analysis of Local Microenvironments in Polymer Films Using Solvatochromic Dyes," *Sensors* 26 (2026): 1346.

37. F. Ito, T. Kakiuchi, T. Sakano, and T. Nagamura, "Fluorescence Properties of Pyrene Derivative Aggregates Formed in Polymer Matrix Depending on Concentration," *Physical Chemistry Chemical Physics* 12 (2010): 10923–10927.

38. C. Würth, M. Grabolle, J. Pauli, M. Spieles, and U. Resch-Genger, "Relative and Absolute Determination of Fluorescence Quantum Yields of Transparent Samples," *Nature Protocols* 8 (2013): 1535–1550.

39. A. M. Brouwer, "Standards for Photoluminescence Quantum Yield Measurements in Solution (IUPAC Technical Report)," *Pure and Applied Chemistry* 83 (2011): 2213–2228.

Supporting Information

Additional supporting information can be found online in the Supporting Information section.